Single Nanoparticle Couplers for Plasmonic Waveguides

*Shunping Zhang, Changzhi Gu, and Hongxing Xu**

Plasmonic waveguides are key elements for highly integrated photonic circuits due to their nanometer-scale footprint thanks to the subwavelength confinement of surface plasmon polaritons (SPPs).[1] The capability of carrying both photonic and electronic signals on the same metallic waveguides is highly attractive especially for nanoscale all-optical or electro-optic devices, such as routers, modulators, inter-connects, and so forth.[2] However, the efficiencies of fueling light into the plasmonic waveguides are quite low due to the impedance mismatch between the waveguides and the free space. For those waveguides with high modal confinement such as metal slot waveguides or thin metal nanowires, typical in-coupling coefficients are only a few percent or smaller even for highly focused light beam illuminating normally onto the input end.[1] On the other hand, the scattering and absorption of light by metal nanoparticles (MNPs) can be significantly enhanced due to the localized surface plasmon resonances (LSPRs).[3] Consequently, MNPs are usually regarded as "optical antennas" for their capability of capturing far-field optical radiation into their close vicinity and vice versa, similar to their radio frequency analogue.[4] A wide range of applications can then be realized using optical antennas, such as surface enhanced spectroscopies,[5] light harvesting,[6] and photodetection.[7] Recently, the idea of using optical antennas as couplers for plasmonic nanocircuits has been exploited.[8–11] For example, asymmetric grating antennas can increase the efficiency of coupling SPPs into a metallic film and improve the directionality.[12] Numerical calculations predicted that a bow-tie antenna can increase the in-coupling efficiency by two orders of magnitude for high confinement slot/gap waveguides under optimized conditions.[8] Later on, experimental realizations were demonstrated successfully for both slot and nanowire waveguides by precisely patterning the antennas.[9] However, the optical antenna couplers reported so far usually have a large size or complicated geometry, for example, Yagi-Uda antennas.[10] The later imposes an increased difficulty in the fabrication process such as precisely aligning the antenna and the waveguide. On the other hand, a randomly attached MNP near a metal film[13] or a nanowire[14] can break the symmetry and mediate the coupling of light into the SPPs. But the efficiency is usually limited because the size and position of the MNP, especially the gap and orientation with respect to the waveguides, can neither be controlled nor optimized.

In this communication, we report a suppression or enhancement of the coupling between SPPs on a metal nanowire and the far-field radiation by a single cut at one end of the nanowire. When thoroughly cut, a self-aligned nanorod-nanowire complex is obtained and the coupling of light into the SPPs on the nanowire is modulated by the LSPRs of the nanorod. For an off-resonant nanorod, the coupling between free space radiation and the nanowire SPPs can be suppressed to about five percent. When partly cut, the created etch can increase the in-coupling efficiency by a factor of 7.7. Such etch-induced in-coupling enhancement is robust to some fabrication errors. Electromagnetic simulations reproduce the observed behaviors and further reveal that the reflectivity of SPPs at the nanowire terminal can be increased (reduced) by the attached off-resonant (resonant) nanorod antenna. This finding paves a simple way to control the coupling efficiency between a plasmonic waveguide and the free space, which is an important aspect in nanophotonic devices. What is more, the cutting-wire scheme can also be extended for more complicated functional device realizations.

Physically, the beauty of using nanorod antennas as nanowire waveguide couplers is schematically shown in **Figure 1**. First, compared with a spherical MNP of the same size, a nanorod has a red-shifted and stronger LSPR, which makes it a more efficient antenna to capture the far-field radiation into its near-field region. More importantly, the far-field radiation pattern of a nanorod is orthogonal to the rod axis while the local electric field is maximized at the two ends. This property maximizes simultaneously the coupling of normally incident far-field light into the nanorod LSPRs and the transfer of nanorod LSPRs into the nanowire SPPs via near-field coupling, as shown in Figure 1A,B. Second, the LSPRs of a nanorod can be simply tuned by varying the rod length.[15] Different order of the longitudinal modes can be viewed as those nanowire SPPs (the fundamental radially polarized mode) that satisfy the resonant conditions of a Fabry-Pérot (FP) cavity between the two end-facets.[16,17] The

Dr. S. Zhang, Prof. C. Gu, Prof. H. Xu
Beijing National Laboratory for Condensed Matter Physics and Institute of Physics
Chinese Academy of Sciences
Box 603–146, Beijing, 100190, China
E-mail: hxxu@aphy.iphy.ac.cn
Dr. S. Zhang, Prof. H. Xu
Center for Nanoscience and Nanotechnology and School of Physics and Technology
Wuhan University
Wuhan 430072, China
Prof. H. Xu
Division of Solid State Physics/The Nanometer Structure Consortium
Lund University
Box 118, S-22100, Lund, Sweden

DOI: 10.1002/smll.201400990

NANO MICRO small

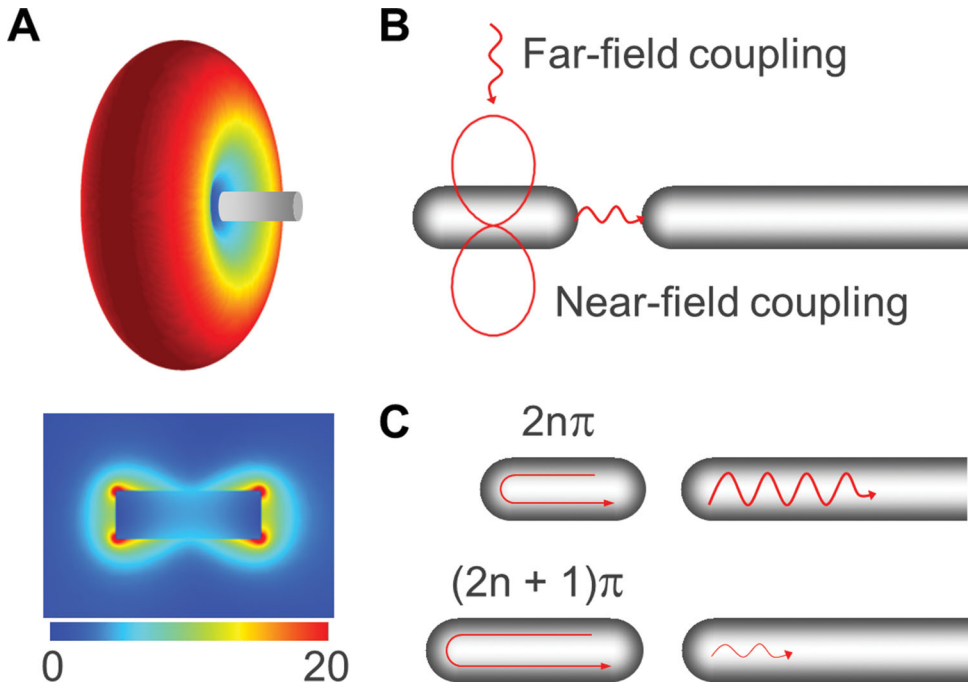

Figure 1. A) Far-field radiation pattern (top) and electric near-field distribution (bottom) of a silver nanorod excited by a plane wave at its LSPR. B) Schematic drawing of a single nanorod coupler benefiting from its far-field and near-field properties. C) Schematic drawing of a resonant and off-resonant nanorod coupler for a nanowire waveguide.

spectral domain between two subsequent resonances, called free spectral range for a conventional FP cavity, defines a window that light cannot pass through. Similarly, this 'forbidden band' for a nanorod can be used to block the SPPs to pass through it. Therefore, the coupling between the light and the SPPs on the nanowire can be easily tuned by the nanorod length, as schematically shown in Figure 1C. From the fabrication point of view, the advantage of using nanorod couplers is that they can be easily realized by using focused ion beam (FIB) to cut at one end of a metallic nanowire. The nanorod and the rest part of the nanowire have the same diameter and are axially self-aligned, which benefits their coupling. What is more, the position and the depth of the cutting gaps can be easily changed during FIB so that the resonant conditions of the nanorod can be finely tuned.

Crystalline Ag nanowires were synthesized following a polyol procedure.[18] The nanowires have a pentagonal cross section with typical diameters around 80 nm. Ag nanowires were dispersed onto a cleaned silicon wafer covered by a thermal oxide (SiO_2) layer of about 300 nm. The choice of silicon substrate satisfies the conductivity required in the FIB experiments while the SiO_2 layer separates the nanowires and the high permittivity silicon to increase the propagation length of the SPPs.[19] An indexed gold/chromium grid was lithographically patterned onto the substrate as markers to identify the measured nanowires in different experiment steps. Coherent white light from a supercontinuum laser (Fianium Ltd.) was focused onto one end of the nanowire by a 100X (N. A. = 0.90) objective. Emission light from the other end of the nanowires was collected by the same objective, dispersed by a 150 lines/mm grating and then recorded by a thermoelectric cooled (–72 °C) CCD (Princeton instrument, PIXIS 256BR). The optical setup is shown in Figure S1 in the Supporting Information. After measuring the transmission spectra, the nanowires were cut by FIB (FEI DB235) at the input end to form a nanorod-nanowire complex. Then, transmission spectra of the same nanowire were measured again. Finally, the geometry of the structure was characterized by scanning electron microscope (SEM). Correlated measurements on a single nanostructure enable us to qualitatively extract the effect of cutting on the optical properties. Since the coupling efficiency is also sensitive to the relative position of the nanowire terminal with respect to the laser focus, it requires that the positions of the sample in the subsequent optical measurements should be the same. To ensure this, the gold index grid was used to align the orientation of the sample with respect to the microscopy. Then, a piezo stage (Nanonics Imaging Co., NIS-70) was used to finely adjust the position of the input end of the nanowire so that the emission from the other end was maximized. All the transmission spectra were subtracted by a background spectra measured at a nearby clean position and then divided by the spectrum of the light source measured from the reflection light of a clean glass substrate using the same optical setup.

Figure 2 shows an example of suppressing light coupling into a Ag nanowire by a cut nanorod. The nanorod was cut with a length of 193 nm and with a gap of 41 nm related to the rest part of the nanowire, as shown in the SEM images in Figure 2A(i,ii). A thin nanowires (D = 94 nm) were chosen to reduce the influence of high order modes that might also be excited by a laser beam focused onto the nanowire terminal.[20] Once excited, SPPs can propagate along the nanowire and emit as photons at the other nanowire terminal. Figure 2A(iii,iv) show the CCD images of the nanowire

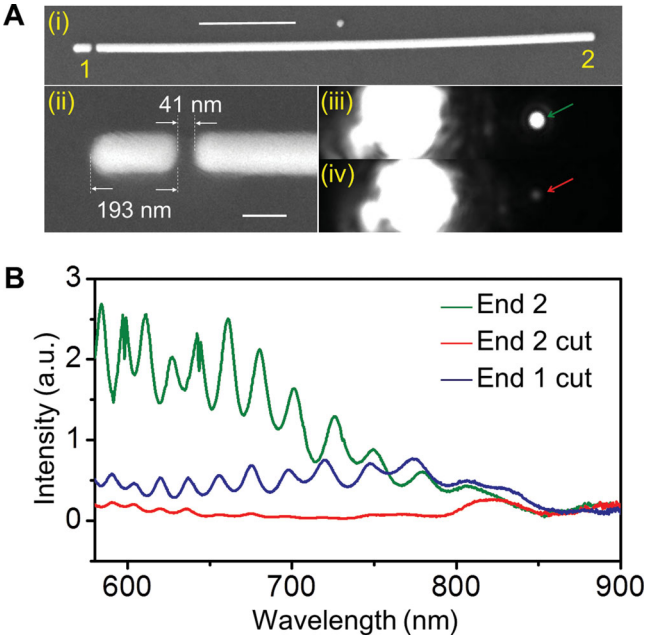

Figure 2. Suppressed nanowire-free space coupling by an off-resonant nanorod. A) SEM (i,ii) and optical (iii,iv) images of a Ag nanorod-nanowire complex fabricated by FIB. Scale bars: 1 μm in (i) and 100 nm in (ii). B) Measured transmission spectra from End 2 of the nanowire before (green) and after (red) cutting. The blue curve shows the transmission from End 1 (using End 2 as input) after cutting.

excited by a supercontinuum laser before and after FIB cutting. Obviously, the transmitted light spot from the output end (End 2) is much brighter before the FIB cut compared with the one after. The spectra of these two transmitted spots were then collected in a confocal manner by a spectrometer, as shown in Figure 2B. Before cutting, significant amount of light covering a broad band can transport through the nanowire. In the near infrared range, the transmitted intensity decreases due to a reduced in-coupling efficiency resulting from the interference of the incident light with the reflected light from the underneath silicon surface.[21] However, with the cut nanorod, the output emission is significantly suppressed over a large spectral range. The ratio of transmitted light after cutting to that before cutting reached a minimum of about 5% near 660 nm. This is because the nanorod plasmon is off-resonant around this region. For wavelength larger than 820 nm, the transmitted intensity is compared to that before cutting. Since the measured nanowire was the same, the propagation loss and the emission efficiency of SPPs into photons at the output end can be assumed to be the same. Therefore, the change in the transmission spectrum should come from the change in the in-coupling efficiency modulated by the nanorod LSPRs.

The Ag nanowire may degrade due to the exposure of the silver metal to the ion beam and the ambient air. To exclude this effect, we measured the transmitted spectrum by using End 2 as input, and collected the emitted light from the cut end (End 1). Shown in Figure 2B, the measured transmission intensity from End 1 was roughly on the same order as that from End 2 before cutting. This confirmed that the Ag nanowire sustained its plasmonic properties during the measurements. A control experiment (Figure S2 in the Supporting Information) further confirmed that the effect of ion beam and ambient air was a minor aspect to explain the suppression of transmission. To exclude the effect of power and spectral stability of the supercontinuum laser, the experiments were also done using a single wavelength He-Ne laser, as shown in Figure S3 (Supporting Information). Despite of fluctuation (likely from the FP resonances on the nanowire), these experiments confirmed that the transmission intensity was suppressed for nanorod with aspect ratio around 2, in agreement with the results in Figure 2 at the wavelength of 632.8 nm.

Another example of cutting nanowire is shown in **Figure 3**A,B. The nanowire had a diameter of 98 nm, a length of 5.75 μm. The cutting gap was 18 nm in width, 296 nm away from the nanowire terminal (see Figure 3A(ii)). But actually, the nanowire was not completely cut – the nanorod and the rest of the nanowire were linked. Different from the previous example, the output emission spot from End 2 became brighter after the FIB cutting, as shown in Figure 3A(iii,iv). Figure 3B confirms that after cutting, the transmitted intensity can be enhanced over the measured spectral range. The ratio of the transmitted intensity (without taking a background subtraction) shows a clear signature of the LSPR of the cut nanowire terminal, with a maximum enhancement factor of 7.7 at 763 nm.[22] The etch-enhanced coupling into the nanowire waveguide can be interpreted as followed. The etch provides a secondary port for light to get into the nanowire. Also, it partly reflects those SPPs excited at the terminal and helps building up the LSPRs of the cut nanowire terminal. Both effects contribute to the enhanced light-SPP coupling for a subwavelength nanowire waveguide. Unlike those nanocouplers making of interacting antennas,[8,9] whose

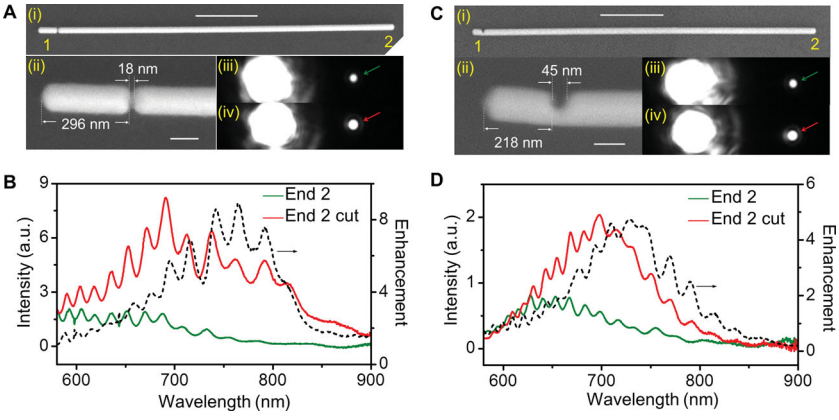

Figure 3. Enhanced coupling of light into a nanowire by a single cut etch. A) (i,ii) SEM images of the cut Ag nanowire; Scale bars: 1 μm in (i) and 100 nm in (ii). iii,iv) Optical images of the nanowire under super-continuum laser excitation before (iii) and after (iv) the FIB cutting. B) Measured transmission spectra of the nanowire before (green solid) and after (red solid) cutting. The black dash line is the ratio of the transmission with and without the cut. C,D) The same as (A,B) but for another nanowire partly cut to the side.

NANO MICRO small

LSPRs depend sensitively on the interparticle gap, the etch-enhanced coupling is more robust to the fabrication deviations. Figures 3C,D show a cut to the side of a nanowire can also increase the in-coupling efficiency. Figure 3C(ii) shows that the etch is 45 nm width, 218 nm away from the nanowire terminal edge. Similarly, the transmission intensity gets enhanced after the FIB cutting, as shown in Figure 3C(iii,iv). Spectral measurements in Figure 3D show a 4.6 times enhancement, with a peak centered at 726 nm. Since the position of the etch determines the length of the 'nanorod', the resonant position is blueshifted compared with the one in Figure 3A. This tunablity paves a simple way to adjust the coupler for a given wavelength.

To confirm and better understand our experimental observations, we performed full-wave electromagnetic simulations using finite-difference time-domain (FDTD) method (Lumerical FDTD Solution). To properly include the effect of substrate,[19,21] we modeled a pentagonal Ag nanowire lying on top of Si–SiO_2 (300 nm) substrate, as shown in **Figure 4**A. The diameter (D = 98 nm) and the length (L = 5.75 μm) corresponded to the measured nanowire shown in Figure 3A. The cut etch was assumed to have a sharp side wall. The optical constants of silicon were adopted from the database by Palik[23] and those for silver were from the experimental data by Johnson and Christy.[24] The refractive index of silicon dioxide was 1.46. The excitation Gaussian beam was polarized along the nanowire axis with a beam width of 0.6 μm. The transmission spectra were calculated by integrating the power flow through a rectangle plane (0.8 μm × 0.8 μm) near the output end of the nanowire. Figure 4B compares the transmission of a Ag nanowire without and with an air etch (cut from the top). In agreement with the experimental observations, the transmission intensity of the nanowire is increased over a broad range of spectrum for the nanowire with a cut etch. The transmission maximum is redshifted from 681 nm to 755 nm. By fitting the transmission power at different position along the nanowire, we can obtain the absolute in-coupling efficiency of light into the nanowire SPPs.[21] The cutting etch can improve the maximum in-coupling efficiency from ≈3.9% to 10.7%. Since the depth of the etch determines the degree the "nanorod" linked to the rest part of the nanowire, it can affect the LSPRs at the cut terminal in a way similar to the loaded nanoantenna.[25] As shown in Figure S4 (Supporting Information), when the etch depth increases from zero to about half of the nanowire diameter, the resonance becomes stronger and the in-coupling efficiency increases. However, as the depth is further increased from half cut to fully cut, the LSPRs vary more dramatically from an enhancement to a suppression in the in-coupling efficiency. The width of the etch, within the experimental obtainable range (about 18 nm to 50 nm) in our study, shows a minor effect on the transmission spectrum for both partly and thoroughly cuts, as shown in Figure S5 (Supporting Information). However, for narrower gaps, the LSPRs of the cut teriminal will change due to the stronger coupling across the gap, which can alter the transmission spectrum of the nanowire accordingly. The focus position of the Gaussian beam, either onto the end of the nanowire or onto the center of the etch, has been tested to have a minor effect on the transmission spectra.

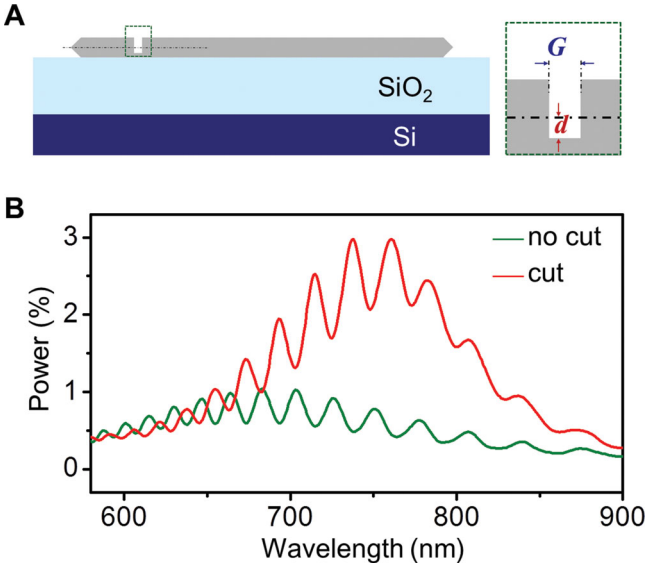

Figure 4. A) Schematically drawing of the geometry used in the calculations (not to scale). B) FDTD calculated transmission spectra of a Ag nanowire without (green) and with (red) a cutting etch. The etch (G = 18 nm, d = –10 nm) is 296 nm away from the tip of the input end.

To further understand the role of nanoantenna on the coupling of light into a nanowire, we turn to an inverse question of how the nanorod modifies the emission properties of SPPs at the nanowire terminal. To simplify the analysis, we focus on an ideal case of a semi-infinitely long nanowire with a cylindrical cross section in homogenous background (air, n_s = 1.0). The calculations were done in two steps using a commercial software (COMSOL Multiphysics 3.5a) based on finite element method (FEM). Briefly, a boundary mode analysis was carried at the input plane on which the radially polarized fundamental mode (TM_0 mode) was picked up and used as the excitation source, see **Figure 5**A. The reflectivity and transmittance of the mode were extracted (see Methods for detailed procedure). Figure 5B shows the end reflectivity of the nanowire terminal (diameter D = 40 nm) can be strongly modulated by the nanorod LSPRs. At the resonant positions, the reflectivity drops to a minimum, meaning that SPPs on nanowire can couple easily into the free-space. Alternatively speaking, the resonant nanorod has a radiative dipolar resonance that can significantly reduce the radiation impedance of the nanowire. However, in the region between different order LSPRs, the reflectivity can be increased compared to the case without the nanorod. For example, at λ = 680 nm, the reflectivity increases from 0.829 for a bare terminal to 0.941 for terminal with an off-resonant nanorod (length L = 200 nm). This makes the off-resonant nanorod a subwavelength reflector. The advantage of nanorod reflector and anti-reflector is their tunablity of the reflection and transmission band by the length of the nanorod. As shown in Figure 5B, the reflection dip shifts from 615 nm (L = 120 nm), to 740 nm (L = 160 nm) and to 865 nm (L = 200 nm). For longer nanorod (L = 240 nm), the second order plasmon resonance appears, with a sharper linewidth due to the smaller radiative damping.[17] Figure 5C shows the electric field and

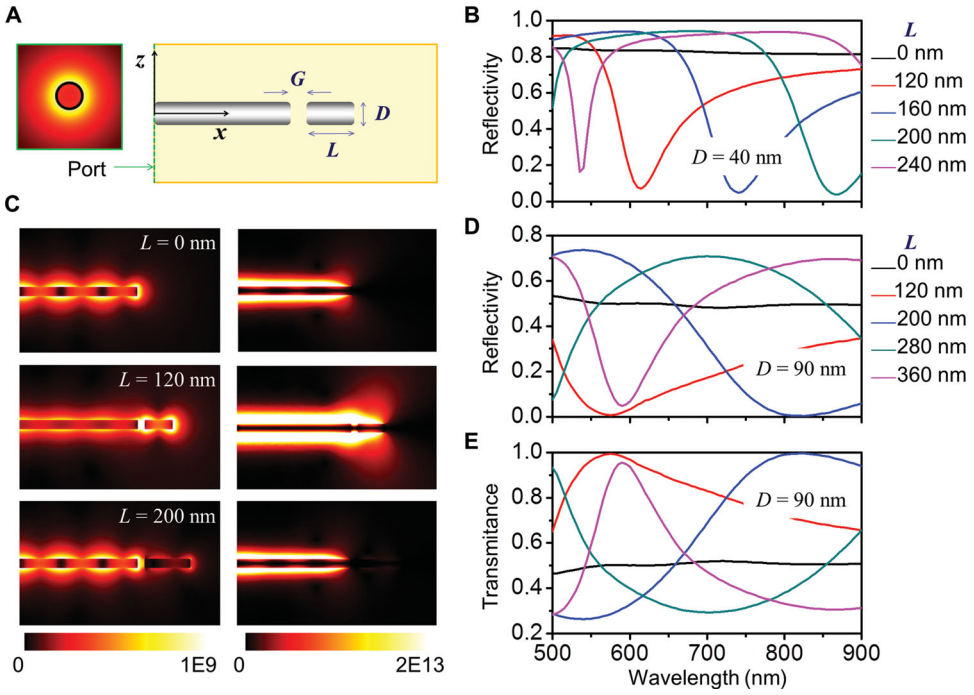

Figure 5. Single nanorod reflector or anti-reflector. A) Schematic drawing of the FEM model using the fundamental nanowire SPP mode as an input excitation. The nanorod (diameter *D*, length *L*) is separated from the nanowire by a gap *G*. The surrounding medium is air. B) The reflectivity of the nanowire-nanorod complex, $D = 40$ nm and $L = 0$ nm, 120 nm, 160 nm, 200 nm, and 240 nm. C) Maps of electric field (left column) and power flow (right column) for vacuum wavelength $\lambda = 615$ nm. D,E) Reflectivity and transmittance of the nanowire-nanorod complex, $D = 90$ nm and $L = 0$ nm, 120 nm, 200 nm, 280 nm, and 360 nm. The nanowire-nanorod separation *G* is 30 nm for all cases.

power flow at the nanowire terminal without and with a nanorod for $\lambda = 615$ nm. For a resonant nanorod ($L = 120$ nm), the reflected SPPs by the terminal is reduced so that the interference pattern on nanowire becomes weak. The power plot shows a stronger emission at the output end. On the contrary, for off-resonant nanorod ($L = 200$ nm), the SPP can hardly couple into the free-space light so that the interference of the incident and reflected SPPs are apparent. Comparing three power plots, it is also clear that the output emission is strongest for a nanowire terminal with a resonant nanorod. Also, the emission angles show a minor change comparing the terminal without or with the resonant nanorod, which further confirms the major role of impedance matching in the above experimental observations. Figure 5D,E shows the reflectivity and transmittance of a thicker nanowire ($D = 90$ nm). For thicker nanowire, the reflectivity at the terminal is about 0.5 for a bare terminal. At the LSPRs of the nanorod, the reflectivity drops down to near zero for the dipolar nanorod LSPR, which corresponds to a nearly unity transmittance as shown in Figure 5E. However, the transmittance ratio (with to without a resonant antenna) become less pronounce for a thick nanowire than for a thin nanowire. This explains why we could not get a large transmission enhancement in the experiments for thoroughly cut nanowires ($D \approx 90$ nm). Therefore, the idea of antenna enhanced in-coupling works better for plasmonic waveguides with higher modal confinement (larger modal mismatch with the free space).

The ability of tuning the reflection/transmission coefficients of the nanowire terminals introduces a way for designing subwavelength nanowire-based positive devices. For example, increasing the transmission coefficients can be used to block the backward reflections or to increase the in-coupling efficiency (demonstrated in this letter). In contrast, increasing the end reflectivity can reduce the cavity losses of the nanowire,[26] a critical issue for tailoring light–matter interaction at the nanoscale.[27] As an example to show the extensibility, Figure S6 (Supporting Information) shows the fabrication of cascaded nanorods at the nanowire terminal. Again, the nanorods are self-aligned and the lengths are fully controllable during FIB. Therefore, the cutting scheme is capable of fabricating some interesting crystallized geometries that are otherwise difficult to realize using bottom up assembly.[28] What is more, the idea of cutting-antenna can be simply extended as efficient nanocouplers for other plasmonic waveguides, nanophotonic circuits, as well as THz devices.

In conclusion, we have introduced an idea of using a compact nanoantenna as coupler for deep subwavelength waveguides. A self-aligned nanorod or a single etch was cut at the input end of a Ag nanowire by FIB. The LSPRs of the nanoantenna can modify the radiation impedance of the nanowire waveguide, which enables the nanoatenna to function as an efficient, compact coupler. By tuning the position of the cut during FIB, the resonant frequencies can be simply controlled. The transmission intensity at the output end of the nanowire can be enhanced (suppressed) with a resonant (off-resonant) nanoantenna at the input end. Electromagnetic simulations reproduced the observed behaviors and confirm the role of radiative dipolar resonance in reducing the impedance mismatch. The resonant (off-resonant) nanorod can function as

small NANO MICRO

a subwavelength anti-reflector (reflector). This study adds to the toolbox for applications in positive plasmonic or nanophotonic components.

Experimental Section

FIB Cutting: To protect the sample, the ion exposure was limited to twice for each nanowire. Under 6.5 k magnification, the sample were identified and moved to the center of the ion beam. Then, the magnification was changed to 35 k under which the nanowires were milled by a line cut. The cutting depth was controlled by a proper combination of the exposure time and the beam current. The acceleration voltage of ion beam was 30 kV and the beam current was 10 pA. Typically, the exposure time ranges from 0.02 s to 0.05 s (also depending on the length of the cut line). We carefully ajusted this exposure time so that no obvious damage to the undernearth silicon dioxide substrate was observed.

Reflection/Transmission Coefficients Calculations using FEM: The calculations were done in two steps. First, a boundary mode analysis was performed at the input port boundary. Second, the fundamental mode was selected and used as excitation source in the following 3D modeling. The calculation domain boundaries were set as scattering boundary condition except the incident plane (port condition). The incident power P_0 was fixed at 1 W. The length of the nanowire L_t was more than 1.75 times the wavelength of the SPP and was adjusted so that the port boundary corresponds to an anti-node of the near-field. The sharp edge of the nanowire terminals and cutting edges had been smoothed by a 2 nm curvature. The propagation length L_{spp} of the selected mode was obtained during mode analysis. The net power through the port plane P_{port} was evaluated by integrating the power density over the plane. The Joule heating P_{heat} along the nanowire was also integrated. Then, the incident power at the terminal was $P_i = P_0 \exp(-L_t/L_{spp})$. The reflected power from the terminal was $P_r = (P_0 - P_{port}) \exp(L_t/L_{spp})$. The transmitted power from the terminal was $P_t = P_{port} - P_{heat}$. Finally, the reflectivity and the transmittance were calculated via $R = P_r/P_i$ and $T = P_t/P_i$. The validity of our calculation results were confirmed by a good agreement with those in the literature.[29]

Supporting Information

Supporting Information is available from the Wiley Online Library or from the author.

Acknowledgements

The authors thank Dr. Yanxue Hou for providing the nanowire sample and thank Dr. Zhipeng Li for helpful discussions. This work was supported by the National Natural Science Foundation of China (Grants Nos. 11304233, 11134013, and 11227407), the Ministry of Science and Technology (Grant No. 2012YQ12006005), "Knowledge Innovation Project" (KJCX2-EW-W04) of CAS and the China Postdoctoral Science Foundation (Grant No. 2013M540596).

[1] D. K. Gramotnev, S. I. Bozhevolnyi, *Nat. Photonics* **2010**, *4*, 83.
[2] a) E. Ozbay, *Science* **2006**, *311*, 189; b) R. Zia, J. A. Schuller, A. Chandran, M. L. Brongersma, *Mater. Today* **2006**, *9*, 20; c) H. Wei, Z. Wang, X. Tian, M. Käll, H. Xu, *Nat. Commun.* **2011**, *2*, 387.
[3] N. J. Halas, S. Lal, W. S. Chang, S. Link, P. Nordlander, *Chem. Rev.* **2011**, *111*, 3913.
[4] a) L. Novotny, N. van Hulst, *Nat. Photonics* **2011**, *5*, 83; b) P. Biagioni, J. S. Huang, B. Hecht, *Rep. Prog. Phys.* **2012**, *75*, 024402.
[5] V. Giannini, A. I. Fernandez-Dominguez, S. C. Heck, S. A. Maier, *Chem. Rev.* **2011**, *111*, 3888.
[6] H. A. Atwater, A. Polman, *Nat. Mater.* **2010**, *9*, 205.
[7] M. W. Knight, H. Sobhani, P. Nordlander, N. J. Halas, *Science* **2011**, *332*, 702.
[8] a) J.-S. Huang, T. Feichtner, P. Biagioni, B. Hecht, *Nano Lett.* **2009**, *9*; b) J. Wen, S. Romanov, U. Peschel, *Opt. Express* **2009**, *17*, 5925.
[9] a) J. Wen, P. Banzer, A. Kriesch, D. Ploss, B. Schmauss, U. Peschel, *Appl. Phys. Lett.* **2011**, *98*, 101109; b) Z. Fang, L. Fan, C. Lin, D. Zhang, A. J. Meixner, X. Zhu, *Nano Lett.* **2011**, *11*, 1676.
[10] A. Kriesch, S. P. Burgos, D. Ploss, H. Pfeifer, H. A. Atwater, U. Peschel, *Nano Lett.* **2013**, *13*, 4539.
[11] A. Alu, N. Engheta, *Phys. Rev. Lett.* **2010**, *104*, 213902.
[12] a) A. Baron, E. Devaux, J.-C. Rodier, J.-P. Hugonin, E. Rousseau, C. Genet, T. W. Ebbesen, P. Lalanne, *Nano Lett.* **2011**, *11*, 4207; b) X. Huang, M. L. Brongersma, *Nano Lett.* **2013**, *13*, 5420.
[13] J. K. Day, O. Neumann, N. K. Grady, N. J. Halas, *ACS Nano* **2010**, *4*, 7566.
[14] a) M. W. Knight, N. K. Grady, R. Bardhan, F. Hao, P. Nordlander, N. J. Halas, *Nano Lett.* **2007**, *7*, 2346; b) B. Kenens, M. Rybachuk, J. Hofkens, H. Uji-i, *J. Phys. Chem. C* **2013**, *117*, 2547.
[15] S. Link, M. B. Mohamed, M. A. El-Sayed, *J. Phys. Chem. B* **1999**, *103*, 3073.
[16] J. Dorfmüller, R. Vogelgesang, R. T. Weitz, C. Rockstuhl, C. Etrich, T. Pertsch, F. Lederer, K. Kern, *Nano Lett.* **2009**, *9*, 2372.
[17] S. Zhang, L. Chen, Y. Huang, H. Xu, *Nanoscale* **2013**, *5*, 6985.
[18] Y. G. Sun, Y. N. Xia, *Adv. Mater.* **2002**, *14*, 833.
[19] S. P. Zhang, H. X. Xu, *ACS Nano* **2012**, *6*, 8128.
[20] S. P. Zhang, H. Wei, K. Bao, U. Håkanson, N. J. Halas, P. Nordlander, H. X. Xu, *Phys. Rev. Lett.* **2011**, *107*, 096801.
[21] Z. P. Li, K. Bao, Y. R. Fang, Z. Q. Guan, N. J. Halas, P. Nordlander, H. X. Xu, *Phys. Rev. B* **2010**, *82*, 241402.
[22] The peak positions and the peak values were obtained after smoothing the Fabry-Pérot ripples by a Fast Fourier Transform filter.
[23] E. D. Palik, *Handbook of Optical Constants of Solids*. Academic Press, New York **1998**.
[24] P. B. Johnson, R. W. Christy, *Phys. Rev. B* **1972**, *6*, 4370.
[25] a) M. Schnell, A. García-Etxarri, A. J. Huber, K. Crozier, J. Aizpurua, R. Hillenbrand, *Nat. Photonics* **2009**, *3*, 287; b) M. Abb, Y. Wang, P. Albella, C. H. de Groot, J. Aizpurua, O. L. Muskens, *ACS Nano* **2012**, *6*, 6462.
[26] H. Ditlbacher, A. Hohenau, D. Wagner, U. Kreibig, M. Rogers, F. Hofer, F. R. Aussenegg, J. R. Krenn, *Phys. Rev. Lett.* **2005**, *95*, 257403.
[27] N. P. de Leon, B. J. Shields, C. L. Yu, D. E. Englund, A. V. Akimov, M. D. Lukin, H. Park, *Phys. Rev. Lett.* **2012**, *108*, 226803.
[28] A. M. Funston, D. E. Gomez, M. Karg, K. C. Vernon, T. J. Davis, P. Mulvaney, *J. Phys. Chem. Lett.* **2013**, *4*, 1994.
[29] S. J. Al-Bader, H. A. Jamid, *Phys. Rev. B* **2007**, *76*, 235410.

Received: April 10, 2014
Revised: June 16, 2014
Published online: July 14, 2014

